PROCEEDINGS OF THE ROYAL SOCIETY A

rspa.royalsocietypublishing.org

Research

Article submitted to journal

Subject Areas:
electromagnetism, wave motion, applied mathematics

Keywords:
Homogenization, metamaterial, effective medium, Bloch modes, Trefftz approximation

Author for correspondence:
Igor Tsukerman
e-mail: igor@uakron.edu

Published in:
Proc.R.Soc.A 470:20140245 (2014)
doi:10.1098/rspa.2014.0245

A nonasymptotic homogenization theory for periodic electromagnetic structures

Igor Tsukerman[1] and Vadim A. Markel[2]

[1]Department of Electrical and Computer Engineering, The University of Akron, OH 44325-3904, USA
[2]Departments of Radiology and Bioengineering and the Graduate Group in Applied Mathematics and Computational Science, University of Pennsylvania, Philadelphia, PA 19104, USA

Homogenization of electromagnetic periodic composites is treated as a two-scale problem and solved by approximating the fields on both scales with eigenmodes that satisfy Maxwell's equations and boundary conditions as accurately as possible. Built into this homogenization methodology is an error indicator whose value characterizes the accuracy of homogenization. The proposed theory allows one to define not only bulk, but also position-dependent material parameters (e.g., in proximity to a physical boundary) and to quantify the trade-off between the accuracy of homogenization and its range of applicability to various illumination conditions.

1. Introduction

Fields scattered by a composite consisting of many elementary cells are difficult to compute. The practical objective of a homogenization theory is to replace the composite with an equivalent homogeneous body that produces approximately the same reflected/transmitted fields. The material tensor $\mathcal{M}$ of this equivalent sample is either constant within its volume or, more generally, is allowed to vary, particularly, near the physical interface. The relevant concept of transition layers has been discussed by Simovski [1,2].

Classical approaches to homogenization are asymptotic (e.g. [3,4]) in the sense that the effective medium parameters are obtained by taking a certain limit. In this paper we propose a novel non-asymptotic effective medium theory.

The term "non-asymptotic" implies that we do not compute a mathematical limit with respect to any physical parameters or combinations thereof; instead, we minimize the errors related to homogenization for a given composition of the material. An important feature of our approach is that it applies to a well-defined range of illumination conditions. Indeed, for a single incident plane wave, it is always possible to find by simple fitting the effective electromagnetic parameters that yield the exact values of the reflection and transmission coefficients, assuming that these quantities can be defined. However, these parameters will not in general be applicable to all possible types of illumination. Our objective is to find parameters that are valid for some range of illumination conditions rather than for a single incident wave. In this case, it is not possible to eliminate homogenization errors altogether but it is possible to minimize them in some sense.

In principle, one can formulate a general optimization problem with respect to the unknown tensor $\mathcal{M}$. In that case, one seeks to minimize the discrepancy between the far fields scattered by the actual and the equivalent samples for various forms of the incident field. This is a nonlinear inverse problem with respect to $\mathcal{M}$. The mainstream approach to solving such problems iteratively is Newton's method [5,6]. We note that, when the incident field is limited to a single plane wave, the inverse problem is of Diophantine type, is ill-posed, and its solution is not unique. This inverse problem has been extensively studied in relation to S-parameter retrieval [7–10]. We have generalized the retrieval procedure to normal and near-normal incidences (Appendix C in [11]), but this development did not eliminate the ill-posedness noted above. Expanding the forward dataset further by including a larger interval of incidence angles is expected to remove the non-uniqueness of the minimizer but will also increase the associated mathematical and computational complexity.

In the present paper, we wish to avoid the global inverse problem. Instead, we seek to define coarse-level fields that coincide with the exact field in the region of measurement outside the material and at the same time satisfy Maxwell's equations in the effective medium approximately but as accurately as practically possible. We propose a specific construction of coarse-level fields leading to a *local* (that is, cell-wise) minimization problem whose object function is quadratic in $\mathcal{M}$, thereby rendering the associated inverse problem linear and directly solvable via the Moore-Penrose pseudoinvese. Both locality and linearity of the problem are essential for making it tractable.

To attain locality, we introduce cell-wise basis sets capable of approximating the fine-level fields with sufficient accuracy. The effective tensor $\mathcal{M}$ can be unambiguously derived from any such basis set using the procedure of Sec. 3. In general, one may choose different bases in different cells and, consequently, the material tensor becomes position-dependent. In some cases, this may have physical significance: for example, near the boundary of the material sample, one may expand the basis by including surface waves [12,13]; this, however, is a separate subject beyond the scope of the present paper. In other cases, discrepancies between the cell-wise material tensors may just be numerical artifacts commensurate with the approximation accuracy; this will happen, for example, if two different Bloch-wave sets are chosen in different cells in the bulk. For maximum generality, we shall append the cell number m as an index to the material tensor $\mathcal{M}_m$. Cells that are similarly situated (e.g., deep in the bulk) should have identical or very close tensors; if that turns out not to be the case in a practical simulation, then either the chosen basis sets have poor approximation properties or the material is not homogenizable under given conditions.

The bases used in this paper consist of so-called Trefftz functions, which, by definition, satisfy the underlying homogeneous differential equation (in electrodynamics, source-free Maxwell's equations). A natural choice of such functions in the bulk of a periodic structure is a set of Bloch waves traveling in different directions, and a natural choice for Trefftz functions in a homogeneous medium is plane waves. We use Trefftz bases because they are known to have good approximation properties. Correspondingly, we will refer to the method proposed here as Trefftz homogenization.

We use the following notation and key assumptions. A periodic composite under consideration is intrinsically linear, scalar and local, and can be characterized by the permittivity $\tilde{\epsilon}(\mathbf{r})$ and

permeability $\tilde{\mu}(\mathbf{r})$. In the remainder, we for simplicity assume that $\tilde{\mu}(\mathbf{r}) \equiv 1$, as is the case at optical frequencies, but extension of our methodology to $\tilde{\mu}(\mathbf{r}) \neq 1$ is straightforward.

The effective parameters will be denoted with ϵ and μ (without the tilde). Both effective parameters ϵ and μ can be different from unity and are, generally, second-rank tensors. We will also include into consideration the effective parameters of magnetoelectric coupling ξ and ζ, so that the effective material tensor is

$$\mathcal{M} \equiv \begin{pmatrix} \epsilon & \xi \\ \zeta & \mu \end{pmatrix} . \tag{1.1}$$

We use calligraphic symbols such as $\mathcal{K}$, $\mathcal{M}$ to denote 6×6 matrices. The tilde sign is used for all lattice-periodic quantities. For example, Bloch-periodic functions (Bloch waves) are written in the form $f(\mathbf{r}) = \tilde{f}(\mathbf{r}) \exp(i\mathbf{q} \cdot \mathbf{r})$, where $\mathbf{q}$ is the Bloch wave vector. For orthorhombic lattices, lattice-periodicity is expressed as

$$\tilde{f}(x + a_x, y + a_y, z + a_z) = \tilde{f}(x, y, z) , \tag{1.2}$$

where a_x, a_y and a_z are the lattice periods. Note that one-dimensional and two-dimensional periodic media can be formally obtained as limits $a_x, a_y \to 0$ or $a_x \to 0$. Of course, in the case of $\tilde{\epsilon}$, the equality (1.2) holds only if the points $\mathbf{r} = (x, y, z)$ and $\mathbf{r}' = (x + a_x, y + a_y, z + a_z)$ are simultaneously located inside the composite or if they are simultaneously located in a vacuum.

Fine-level fields – that is, the exact solutions to macroscopic Maxwell's equations – are denoted with small letters $\mathbf{e}$, $\mathbf{d}$, $\mathbf{h}$ and $\mathbf{b}$. Capital letters $\mathbf{E}$, $\mathbf{D}$, $\mathbf{H}$, $\mathbf{B}$ are used for coarse-level fields that vary on a scale larger than the cell size. The quantities $\mathbf{e}$, $\mathbf{d}$, $\mathbf{h}$ and $\mathbf{b}$ should not be confused with the fields of microscopic electrodynamics. It is important to keep this distinction in mind because the notations utilizing small letters for the *microscopic* (atomic-level) electromagnetic fields are customarily used in textbooks and papers that derive macroscopic Maxwell's equations from the atomic-level fields. However, in this paper, we consider a different problem and do not go outside of the theoretical framework of macroscopic electrodynamics. Thus, fine-level fields are assumed to satisfy the constitutive relations

$$\mathbf{d}(\mathbf{r}) = \tilde{\epsilon}(\mathbf{r})\mathbf{e}(\mathbf{r}) , \quad \mathbf{b}(\mathbf{r}) = \mathbf{h}(\mathbf{r}) . \tag{1.3}$$

Note that $\mathbf{h}(\mathbf{r}) = \mathbf{b}(\mathbf{r})$ because the medium is assumed to be intrinsically nonmagnetic.

The electromagnetic problem is formulated in in the frequency domain with the $\exp(-i\omega t)$ phasor convention. At a working frequency ω, the free-space wave number $k_0 = \omega/c = 2\pi/\lambda$, where λ is the free-space wavelength.

2. Formulation of the problem

A theory of homogenization is only physically interesting if it can describe finite samples; we have discussed this in detail in [11]. In this paper, we develop a theory that is applicable to finite samples of reasonably "simple" shape. We do not define this requirement of "simplicity" precisely but note that the theory might break, for example, for samples that are not convex or contain internal voids. However, the theory should, at least, be applicable to slabs of finite width. Correspondingly, we will focus on this physical object in the remainder of the paper. This will allow us to avoid the complicated issues related to the behavior of fields near edges and corners. We note that applications of metamaterial slabs have been proposed in relation to imaging beyond the diffraction limit [14].

Thus, in what follows, we assume that a periodic composite (a photonic crystal) is contained between the planes $z = 0$ and $z = L$. The fine-level fields satisfy macroscopic Maxwell's equations of the form

$$\nabla \times \mathbf{h}(\mathbf{r}) = -ik_0\tilde{\varepsilon}(\mathbf{r})\mathbf{e}(\mathbf{r}) , \quad \nabla \times \mathbf{e}(\mathbf{r}) = ik_0\mathbf{h}(\mathbf{r}) \tag{2.1}$$

everywhere in space, supplemented by the usual radiation boundary conditions at infinity. Outside of the slab, the most general solution to (2.1) can be written as a superposition of

incident, transmitted and reflected waves. For the electric field, we can write these in the form of angular-spectrum expansions:

$$\mathbf{e}_i(\mathbf{r}) = \int \mathbf{s}_i(k_x, k_y) e^{i(k_x x + k_y y + k_z z)} dk_x dk_y \,, \tag{2.2a}$$

$$\mathbf{e}_t(\mathbf{r}) = \int \mathbf{s}_t(k_x, k_y) e^{i(k_x x + k_y y + k_z z)} dk_x dk_y \,, \quad z > L \,, \tag{2.2b}$$

$$\mathbf{e}_r(\mathbf{r}) = \int \mathbf{s}_r(k_x, k_y) e^{i(k_x x + k_y y - k_z z)} dk_x dk_y \,, \quad z < 0 \,, \tag{2.2c}$$

where

$$k_z = \sqrt{k_0^2 - k_x^2 - k_y^2} \,, \tag{2.3}$$

and the square root branch is defined by the condition $0 \leq \arg(k_z) < \pi$. Expressions for the magnetic field are obtained from (2.2) by using the second Maxwell equation in (2.1). In (2.2), $\mathbf{s}_i(k_x, k_y)$, $\mathbf{s}_t(k_x, k_y)$ and $\mathbf{s}_r(k_x, k_y)$ are the angular spectra of the incident, transmitted and reflected fields. Waves included in these expansions can be both evanescent and propagating. For propagating waves, $k_x^2 + k_y^2 < k_0^2$, otherwise the waves are evanescent. (Note that the operation of the so-called superlens [14] implies amplified transmission of exponentially weak evanescent waves.)

Everywhere in space, the total electric field $\mathbf{e}(\mathbf{r})$ can be written as a superposition of the incident and scattered fields, viz,

$$\mathbf{e}(\mathbf{r}) = \mathbf{e}_i(\mathbf{r}) + \mathbf{e}_s(\mathbf{r}) \,. \tag{2.4}$$

Outside of the material, the reflected and transmitted fields form the scattered field:

$$\mathbf{e}_s(\mathbf{r}) = \begin{cases} \mathbf{e}_r(\mathbf{r}) \,, & z < 0 \,, \\ \mathbf{e}_t(\mathbf{r}) \,, & z > L \,. \end{cases} \tag{2.5}$$

The scattered field *inside* the material is also formally defined by (2.4).

We note that in the case of homogeneous slabs, a single incident plane wave gives rise to one reflected and one transmitted plane wave; the projections of the wave vectors of all three waves onto the interface are in this case equal. For composite slabs, this is not generally so because of the presence of complicated surface waves [11]. If the lattice periods (in the X- and Y-directions) are smaller than λ, the surface waves are exponentially localized near the physical interface. However, if this condition is violated, the surface waves become propagating in free space, which gives rise to Bragg diffraction and reflection and a number of secondary maxima in the transmitted and reflected angular spectra. Under these conditions, homogenization can only be treated in a very special sense, defined by Craster *et al.* [15,16]; this is beyond the scope of the present paper. We restrict attention to the region of parameters $a_x, a_y < \lambda$, although we do not require that this inequality hold strongly.

3. Nonasymptotic (Trefftz) homogenization

In what follows, we introduce an approximation of the fine-scale fields and a procedure for constructing auxiliary coarse-level fields from the former. Identifying and minimizing the approximation errors is inherent in this procedure. We will finally define the effective material tensor.

(a) Approximation of fine-scale fields

Fine-scale fields can be approximated using a suitable finite set of basis functions. To make the procedure practical, we choose local basis functions $\psi_{m\alpha}$ which are supported cell-wise:

$$\psi_{m\alpha}(\mathbf{r}) = \begin{cases} \{\mathbf{e}_{m\alpha}(\mathbf{r}), \mathbf{h}_{m\alpha}(\mathbf{r})\} \,, & \mathbf{r} \in \mathbb{C}_m \,, \\ 0 \,, & \mathbf{r} \notin \mathbb{C}_m \,. \end{cases} \tag{3.1}$$

Here $\mathbb{C}_m$ is the m-th open lattice cell and index α labels the basis functions supported in $\mathbb{C}_m$. The significance of introducing the locally-supported basis functions will soon become apparent. In principle, the number n of basis functions may be different in different cells, but for notational simplicity this is not explicitly indicated. We also tacitly assume that the basis functions have the level of smoothness required for all stages of our analysis.

The fine-scale field $\psi \equiv \{\mathbf{e}(\mathbf{r}), \mathbf{h}(\mathbf{r})\}$ can be expanded in the given basis as

$$\psi(\mathbf{r}) = \sum_{\alpha,m} c_{m\alpha}\psi_{m\alpha}(\mathbf{r}) + \delta(\mathbf{r}) \,, \tag{3.2}$$

where the term δ represents the approximation error referred to as the "out-of-the-basis error" in [17–19] and $c_{m\alpha}$ are expansion coefficients. We expect that the basis contains enough functions so that δ is small. Note that expansion (3.2) applies to any point inside the material. The proposed homogenization procedure relies only on the basis set itself, not on the expansion coefficients.

To construct a basis set with good approximation properties, we use Trefftz functions, that is, waves that satisfy homogeneous Maxwell's equations in a given cell. Bloch waves propagating in various directions are a particular example of Trefftz functions. While mathematical issues related to convergence of Trefftz approximations are quite technical [20–22], there is ample evidence in the literature that the approximation errors are reasonably low even for bases of small size [20,21, 23,24], as long as the illumination conditions are within a certain range. For example, consider any Maxwellian field that results from illumination of a composite slab by an arbitrary superposition of plane waves with any incidence angles in the range $[-\theta_{\max}, \theta_{\max}]$. Such a field can be expanded (in any given cell) with good accuracy into a basis of n local Trefftz functions corresponding to n incident plane waves with discrete incidence angles varying from $-\theta_{\max}$ to $\theta_{\max}$. If we restrict consideration to propagating incident waves only, a good approximation can often be obtained with only 8 Trefftz functions in 2D or 12 functions in 3D [23–25].

In the remainder, we shall assume that the basis defined in (3.1) and (3.2) consists of Bloch waves

$$\mathbf{e}_\alpha(\mathbf{r}) = \tilde{\mathbf{e}}_\alpha(\mathbf{r}) \exp(i\mathbf{q}_\alpha \cdot \mathbf{r}) \,, \quad \mathbf{h}_\alpha(\mathbf{r}) = \tilde{\mathbf{h}}_\alpha(\mathbf{r}) \exp(i\mathbf{q}_\alpha \cdot \mathbf{r}) \,, \tag{3.3}$$

where the index α labels both the wave vector and the polarization state of the Bloch wave (at a given frequency); $\tilde{\mathbf{e}}_\alpha(\mathbf{r})$, $\tilde{\mathbf{h}}_\alpha(\mathbf{r})$ are the lattice-periodic factors of the respective Bloch waves. Thus, the Trefftz basis set we are using is

$$\psi_{m\alpha}(\mathbf{r}) = \begin{cases} \{\tilde{\mathbf{e}}_\alpha(\mathbf{r}), \tilde{\mathbf{h}}_\alpha(\mathbf{r})\} e^{i\mathbf{q}_{m\alpha}\cdot\mathbf{r}} \,, & \mathbf{r} \in \mathbb{C}_m \,, \\ 0 & \mathbf{r} \notin \mathbb{C}_m \,. \end{cases} \tag{3.4}$$

It is assumed that, for practical purposes, the Bloch modes can be computed numerically.

(b) Approximation of coarse-level fields

We now describe the construction of coarse-level fields $\mathbf{E}$ and $\mathbf{H}$ from $\mathbf{e}$ and $\mathbf{h}$. As above, the coarse-level fields will be expanded in a finite set of Trefftz functions, which in the case of a homogeneous equivalent medium are just plane waves. Two constraints on the definition of the coarse fields are central in the analysis below.

First, we require that the coarse-level fields satisfy Maxwell's equations with an effective material tensor $\mathcal{M}_m$ approximately but accurately. This is expressed as

$$\delta\mathbf{J}_m(\mathbf{r}) = \nabla \times \mathbf{H}(\mathbf{r}) + ik_0\mathbf{D}(\mathbf{r}) \,, \qquad \mathbf{r} \in \mathbb{C}_m \,, \tag{3.5a}$$

$$\delta\mathbf{I}_m(\mathbf{r}) = \nabla \times \mathbf{E}(\mathbf{r}) - ik_0\mathbf{B}(\mathbf{r}) \,, \qquad \mathbf{r} \in \mathbb{C}_m \,, \tag{3.5b}$$

$$\delta\mathbf{K}_{lm}(\mathbf{r}) = \hat{\mathbf{n}}_{lm} \times [\mathbf{H}_l(\mathbf{r}) - \mathbf{H}_m(\mathbf{r})] \,, \qquad \mathbf{r} \in \mathbb{S}_{lm} \,, \tag{3.5c}$$

$$\delta\mathbf{Q}_{lm}(\mathbf{r}) = \hat{\mathbf{n}}_{lm} \times [\mathbf{E}_l(\mathbf{r}) - \mathbf{E}_m(\mathbf{r})] \,, \qquad \mathbf{r} \in \mathbb{S}_{lm} \,, \tag{3.5d}$$

$$\{\mathbf{D}(\mathbf{r}), \mathbf{B}(\mathbf{r})\} = \begin{cases} \mathcal{M}_m\{\mathbf{E}(\mathbf{r}), \mathbf{H}(\mathbf{r})\} \,, & \mathbf{r} \in \mathbb{C}_m \,, \\ \{\mathbf{E}(\mathbf{r}), \mathbf{H}(\mathbf{r})\} \,, & z \notin [0, L] \,, \end{cases} \tag{3.5e}$$

where $\mathbb{C}_m$ is the m-th open cell and $\hat{\mathbf{n}}_{lm}$ is the unit normal on the interface between the two neighboring cells $\mathbb{C}_l$ and $\mathbb{C}_m$, pointing from $\mathbb{C}_l$ to $\mathbb{C}_m$, and the subscripts l and m refer to the fields on each side of the boundary when approaching from the interior of the l-th and m-th cells. Here the terms $\delta\mathbf{J}_m$, $\delta\mathbf{I}_m$, $\delta\mathbf{K}_{lm}$ and $\delta\mathbf{Q}_{lm}$ can be interpreted as spurious volume and surface currents of the electric and magnetic charge. The surface currents are supported on $\mathbb{S}_{lm}$. These currents are not physically present in the medium but simply represent approximation errors. Importantly, $\delta\mathbf{K}_{lm}$ and $\delta\mathbf{Q}_{lm}$ can exist also on the interface between a given cell and empty space, if this cell is located at the outer boundary of the periodic structure. For uniformity of notation, the two half-spaces $z<0$ and $z>L$ can be regarded as two "nonstandard cells" and are denoted here by $\mathbb{C}_0$ and $\mathbb{C}_\infty$, respectively. The interfaces between the boundary layer cells and $\mathbb{C}_0$ and $\mathbb{C}_\infty$ are denoted with $\mathbb{S}_{0m}$ and $\mathbb{S}_{m\infty}$. Then expressions (3.5*c*), (3.5*d*) apply to the interfaces between the "non-standard" and "standard" cells without exceptions. Note that the material tensor $\mathcal{M}_m$ appearing in (3.5*e*) will be determined by minimizing the error terms $\delta\mathbf{J}_m$, $\delta\mathbf{I}_m$, $\delta\mathbf{K}_{lm}$ and $\delta\mathbf{Q}_{lm}$.

The second constraint on the coarse fields is that they must be close to the exact fine-scale fields in the far-field zone of the sample. In practice, the fine-scale and coarse-scale fields should coincide in the region of space where the measurements are made. However, such equality cannot hold in principle if the observation point is located too close to the surface of the composite. Indeed, recall that a three-dimensional composites support a complicated surface wave which has spatial Fourier harmonics with the wave numbers $2\pi(n_x/a_x+n_y/a_y)$, where n_x and n_y are nonzero integers. The coarse-level fields do not contain such high-frequency components. Luckily, the surface wave is evanescent and decays on the scale of $\max(a_x,a_y)/2\pi$. We can, therefore, write the coarse-level electric field in an angular-spectrum expansion form similar to (2.2):

$$\mathbf{E}(\mathbf{r})=\begin{cases}\mathbf{e}_i(\mathbf{r})+\mathbf{E}_r(\mathbf{r})\,, & z<0\,,\\ \mathbf{E}_t(\mathbf{r})\,, & z<L\,,\end{cases} \tag{3.6}$$

where we have assumed that the incident component is the same for the coarse- and fine-scale fields: $\mathbf{e}_i(\mathbf{r})\equiv\mathbf{E}_i(\mathbf{r})$. Then the reflected and transmitted components of the coarse-level field can be expanded as

$$\mathbf{E}_t(\mathbf{r})=\int\mathbf{S}_t(k_x,k_y)e^{i(k_xx+k_yy+k_zz)}\,dk_x\,dk_y\,,\quad z>L\,, \tag{3.7a}$$

$$\mathbf{E}_r(\mathbf{r})=\int\mathbf{S}_r(k_x,k_y)e^{i(k_xx+k_yy-k_zz)}\,dk_x\,dk_y\,,\quad z<0\,, \tag{3.7b}$$

where k_z obeys the free-space dispersion relation (2.3). Now the constraint on the coarse-level field can be formulated as

$$\Theta(k_x,k_y)\,[\mathbf{S}_{r,t}(k_x,k_y)-\mathbf{s}_{r,t}(k_x,k_y)]=0\,, \tag{3.8}$$

where $\Theta(k_x,k_y)$ is a low-pass filtering function. In the simplest case, we can take $\Theta(k_x,k_y)$ to be a unit step function in 2D Fourier space, equal to zero if $|k_{x,y}|>\beta k_0$ and to unity otherwise, where β determines the bandwidth. Homogenization is physically reasonable if we can choose $1<\beta<\lambda/\max(a_x,a_y)$. As was noted above, if $\lambda<\max(a_x,a_y)$, a single reflected or transmitted plane wave can not be defined even under illumination by a single plane wave; homogenization is impossible in this case.

We are now ready to define the coarse-level fields that satisfy the above requirements. In free space, we take (3.8) as a definition of the coarse field. The spectrum of the coarse field outside the filtering window $|k_{x,y}|>\beta k_0$ can be set to zero. Inside the material, we define these fields in a manner similar to (3.2), except that, instead of Bloch waves, we use plane-wave eigenmodes $\Psi_{m\alpha}=\{\mathbf{E}_{m\alpha},\mathbf{H}_{m\alpha}\}$ of Maxwell's equations in a homogeneous but possibly anisotropic medium. For the abstract vector of the coarse field $\Psi=\{\mathbf{E},\mathbf{H}\}$, we can write the cell-wise expansion

$$\Psi(\mathbf{r})=\sum_\alpha c_{m\alpha}\Psi_{m\alpha}(\mathbf{r})\,,\quad \Psi_{m\alpha}(\mathbf{r})\equiv\{\mathbf{E}^{(0)}_{m\alpha},\mathbf{H}^{(0)}_{m\alpha}\}\exp(i\mathbf{q}_{m\alpha}\cdot\mathbf{r})\,,\quad \mathbf{r}\in\mathbb{C}_m\,, \tag{3.9}$$

where the amplitudes $\{\mathbf{E}^{(0)}_{m\alpha},\mathbf{H}^{(0)}_{m\alpha}\}$ are yet to be determined.

Since (3.9) is taken as a definition of coarse-level fields, there is no approximation error associated with this expansion. Thus, each Trefftz basis function for the coarse-level fields is a plane wave with the wave vector $\mathbf{q}_{m\alpha}$, chosen to be the same as the Bloch wave vector in (3.4). This is, indeed, a necessary condition for the discrepancies in (3.5) to be minimized. Physically, this condition requires that the dispersion relations in the effective and exact media be approximately the same.

(More precisely, the wave vector of the plane wave in (3.9) should correspond to that of the dominant plane-wave harmonic of the Bloch wave in (3.4); that is, the $\mathbf{q}_{m\alpha}$ in (3.4) and (3.9) may not necessarily be the same and may in general differ by a reciprocal lattice vector $(2\pi m_x/a_x, 2\pi m_y/a_y, 2\pi m_z/a_z)$ for some integers (m_x, m_y, m_z). For simplicity of notation, though, we tacitly assume that the dominant plane-wave harmonic of the Bloch wave is in the first Brillouin zone, in which case the $\mathbf{q}_{m\alpha}$ in (3.4) and (3.9) are indeed identical.)

Expansion (3.9) can now be substituted into the coarse-field equations (3.5*a*), (3.5*b*). The resultant expressions are given in the Appendix; but the homogenization procedure can be explained without making explicit use of these expressions. Our key objective is to minimize the error fields resulting from both surface and volume error terms (3.5), with the coarse-level fields expanded as (3.9). Some of the parameters of this problem are under our control, while others are not; minimization will obviously be carried out with respect to the former. Parameters that can*not* be controlled include Bloch vectors $\mathbf{q}_{m\alpha}$ (which depend entirely on the given microstructure of the cell) and the expansion coefficients $c_{m\alpha}$ (which depend on the actual fine-level field and are in general unknown). Minimization is to be carried out with respect to the material tensor $\mathcal{M}_m$ and the corresponding amplitudes $\{\mathbf{E}^{(0)}_{m\alpha}, \mathbf{H}^{(0)}_{m\alpha}\}$ of the coarse-level plane waves.

The minimization problem in the form outlined above is intractable due to several complications: (i) the fields in all lattice cells are coupled (because of interface continuity conditions); (ii) effects of both surface and volume error terms are also coupled; (iii) the expansion coefficients $c_{m\alpha}$ are unknown.

The problem can be dramatically simplified, however. Indeed, there is no need to look for a global or even a local minimum; all that's needed is a practical procedure leading to small (but not necessarily the smallest possible) errors and a reasonable estimate of these errors. Accordingly, all references to error "minimization" in this paper should be understood in the above broad sense, i.e., as a practical procedure leading to sufficiently small errors rather than to the absolute minimum.

With this in mind, the obstacles (i)-(iii) above can be removed. Our first consideration is (i): to make error minimization practical, we wish to reduce it to a local (cell-wise) problem. This is easily done by noting that at each interface (cell/cell or cell/air), the triangle inequality

$$\|\delta\mathbf{Q}_{lm}\| = \|\hat{\mathbf{n}}_{lm} \times (\mathbf{E}_l - \mathbf{E}_m)\,\| \;\le\; \|\hat{\mathbf{n}}_{lm} \times (\mathbf{E}_l - \mathbf{e})\,\| + \|\hat{\mathbf{n}}_{lm} \times (\mathbf{E}_m - \mathbf{e})\,\| \quad \text{on } \mathbb{S}_{lm}\,, \tag{3.10}$$

holds, where $\|\cdot\|$ is the L_2-norm. A similar inequality applies to the magnetic field. Thus, if the discrepancy between each coarse field and the exact field at the boundary is sufficiently small, so is the discrepancy between the coarse fields across this boundary. Hence we shall simply seek to minimize the former.

This immediately brings us to item (ii). Even though simultaneous minimization of the surface and volume error terms appears to be an intractable problem, we propose a two-step minimization where the surface error-currents are minimized first, using (3.10), and the volume currents second.

Finally, with regard to the unknown expansion coefficients $c_{m\alpha}$ [item (iii)], we note that the difference between the coarse and fine fields can be written via the modal expansion as

$$\Big\| \sum_\alpha c_{m\alpha}(\Psi_{m\alpha} - \psi_{m\alpha}) \Big\| \;\le\; C \left(\sum_\alpha \|\Psi_{m\alpha} - \psi_{m\alpha}\|^2 \right)^{\frac{1}{2}}, \quad \forall m\,, \tag{3.11}$$

where C is an upper bound for $\|c_m\|$, and $c_m \equiv (c_{m1}, c_{m2}, \ldots, c_{mn})^T$. [1] If the right hand side of (3.11), which can be interpreted as an average errors for all modes, is small, so is the left hand side. This allows us to focus on minimizing the average and remove the unknown coefficient vector c_m from consideration.

Now that the key ideas have been fixed, we are ready to formulate the homogenization procedure.

(c) Maximizing the accuracy of effective medium description

We now seek the effective tensors $\mathcal{M}_m$ and the field amplitudes $\{\mathbf{E}^{(0)}_{m\alpha}, \mathbf{H}^{(0)}_{m\alpha}\}$ that minimize the error terms in (3.5*c*), (3.5*d*). The procedure consists of two steps. In Step 1, we minimize the surface terms $\delta\mathbf{K}_{lm}$ and $\delta\mathbf{Q}_{lm}$ defined by (3.5). In Step 2, we minimize the volume currents $\delta\mathbf{J}_m$ and $\delta\mathbf{I}_m$ defined by (3.5*a*), (3.5*b*). Once this is done, the residual error serves as an overall error indicator.

Step 1. To make $\delta\mathbf{K}_{lm}$, $\delta\mathbf{Q}_{lm}$ as small as possible, one needs to minimize the discrepancies between the tangential components of $\mathbf{E}$ and $\mathbf{H}$ across all cell boundaries (and most importantly, across the material/air interface). As already noted, we avoid this global problem by minimizing, for each cell boundary $\partial\mathbb{C}_m$, the discrepancy between the coarse fields and the respective fine-scale fields rather than between the coarse fields on the two sides of the boundary:

$$\min_{\mathbf{E}^{(0)}_{m\alpha}, \mathbf{H}^{(0)}_{m\alpha}} \left\{ \left\| \hat{\mathbf{n}} \times (\mathbf{E}_{m\alpha} - \mathbf{e}_{m\alpha}) \right\|_{\partial\mathbb{C}_m} + \left\| \hat{\mathbf{n}} \times (\mathbf{H}_{m\alpha} - \mathbf{h}_{m\alpha}) \right\|_{\partial\mathbb{C}_m} \right\} , \tag{3.12}$$

where $\|\cdot\|$ is the L_2-norm. More precisely, one observes that if the norms in (3.12) are sufficiently small, so are the surface error terms $\delta\mathbf{Q}_{lm}$, $\delta\mathbf{K}_{lm}$. Indeed, the first term in the right hand side of (3.10) can be related to the respective term in (3.12) via

$$\begin{aligned} \left\| \hat{\mathbf{n}}_{lm} \times (\mathbf{E}_m - \mathbf{e}) \right\|_{\mathbb{S}_{lm}} &= \left\| \hat{\mathbf{n}}_{lm} \times \left(\sum_\alpha c_{m\alpha} (\mathbf{E}_{m\alpha} - \mathbf{e}_{m\alpha}) + \delta \right) \right\|_{\mathbb{S}_{lm}} \\ &\le C \left(\sum_\alpha \left\| \hat{\mathbf{n}}_{lm} \times (\mathbf{E}_{m\alpha} - \mathbf{e}_{m\alpha}) \right\|^2_{\partial\mathbb{C}_m} \right)^{1/2} + \|\hat{\mathbf{n}}_{lm} \times \delta\|_{\partial\mathbb{C}_m} , \end{aligned} \tag{3.13}$$

where we used approximation (3.2) of the fine-scale fields and the obvious fact that the norm over part of the cell boundary cannot exceed the norm over the whole boundary. Clearly, similar considerations apply to the second terms in (3.10) and (3.12).

In (3.12) we have defined a quadratic minimization problem with respect to the vector amplitudes $\mathbf{E}^{(0)}_{m\alpha}$, $\mathbf{H}^{(0)}_{m\alpha}$. Its solution for cell $\mathbb{C}_m$ of arbitrary shape (not necessarily hexahedral) can be written as

$$\mathbf{E}^{(0)}_{m\alpha} = \left(\int_{\partial\mathbb{C}_m} \mathcal{N}^T(\mathbf{r}) \mathcal{N}(\mathbf{r}) dS \right)^{-1} \int_{\partial\mathbb{C}_m} \mathcal{N}^T(\mathbf{r}) \mathcal{N}(\mathbf{r})\, \tilde{\mathbf{e}}_{m\alpha} dS , \tag{3.14a}$$

$$\mathbf{H}^{(0)}_{m\alpha} = \left(\int_{\partial\mathbb{C}_m} \mathcal{N}^T(\mathbf{r}) \mathcal{N}(\mathbf{r}) dS \right)^{-1} \int_{\partial\mathbb{C}_m} \mathcal{N}^T(\mathbf{r}) \mathcal{N}(\mathbf{r})\, \tilde{\mathbf{h}}_{m\alpha} dS , \tag{3.14b}$$

where $\mathcal{N}(\mathbf{r})$ is a 3×3 matrix representing $\hat{\mathbf{n}}(\mathbf{r})\times$ in the Cartesian system. For hexahedral cells, (3.14*a*) and (3.14*b*) simplify to

$$\mathbf{E}^{(0)}_{m\alpha x} = \int_{\partial\mathbb{C}_{mx}} \tilde{\mathbf{e}}_{m\alpha x}\, dS , \quad \mathbf{H}^{(0)}_{m\alpha} = \int_{\partial\mathbb{C}_{mx}} \tilde{\mathbf{h}}_{m\alpha x}\, dS , \tag{3.15}$$

with similar expressions for the y and z components. Here $\partial\mathbb{C}_{mx}$ denotes part of the cell boundary (four faces) parallel to the x-axis. Note that the averages above involve the periodic factor of the Bloch wave.

[1] This slight generalization of the Cauchy-Schwarz inequality can be proved e.g. by noting that, for any coefficients a_α and functions $g_\alpha(\mathbf{r})$, $\|\sum_\alpha a_\alpha g_\alpha(\mathbf{r})\|^2 = (Ga, a) \le \lambda_{\max}(G)\|a\|^2$, G being the Gram matrix of the set $\{g_\alpha\}$, and then estimating the maximum eigenvalue $\lambda_{\max}(G)$ via the trace of G.

This completes Step 1 of the procedure: the surface error terms $\delta\mathbf{K}_{lm}$, $\delta\mathbf{Q}_{lm}$ have been minimized. We therefore define the coarse-level basis as plane waves (3.9) with the amplitudes $\{\mathbf{E}^{(0)}_{m\alpha}, \mathbf{H}^{(0)}_{m\alpha}\}$ defined by (3.15).

Step 2. The next step of our procedure involves a minimization problem for the volume error terms in (3.5*a*), (3.5*b*):

$$\min_{\mathcal{M}_m} \sum_{\alpha} \left\| \mathcal{K}_{m\alpha}\{\mathbf{H}^{(0)}_{m\alpha}, \mathbf{E}^{(0)}_{m\alpha}\} - k_0 \mathcal{M}_m \{\mathbf{E}^{(0)}_{m\alpha}, \mathbf{H}^{(0)}_{m\alpha}\} \right\|^2 , \tag{3.16}$$

where

$$\mathcal{K}_{m\alpha} \equiv \begin{pmatrix} -\mathbf{q}_{m\alpha}\times & 0 \\ 0 & \mathbf{q}_{m\alpha}\times \end{pmatrix} \tag{3.17}$$

and $\mathbf{q}\times$ is the matrix representation of the cross product with $\mathbf{q}$.

This problem is not only tractable but has a closed-form solution for the entries of the material tensor $\mathcal{M}_m$. Indeed, note that the functional in (3.16) is quadratic with respect to these entries. Minimization of this quadratic functional for a generic material tensor is straightforward; it takes on a particularly simple form if the tensor is known *a priori* to be diagonal (e.g., from symmetry considerations), $\mathcal{M}_m = \mathrm{diag}(\epsilon_{m,xx}, \epsilon_{m,yy}, \epsilon_{m,zz}, \mu_{m,xx}, \mu_{m,yy}, \mu_{m,zz})$. Then in the minimization problem the entries of the tensor decouple. For example, we obtain the following minimization problem for the components of the permeability:

$$\min_{\mu_{m,xx}} \sum_{\alpha} \left| k_0 \mu_{m,xx}[h_{m,\alpha x}] - (\mathbf{q}_{m\alpha} \times [\mathbf{e}_{m,\alpha}])_x \right|^2 \tag{3.18}$$

with analogous problems for the yy and zz components. For the permittivity tensor, the minimization problem is very similar:

$$\min_{\epsilon_{m,xx}} \sum_{\alpha} \left| k_0 \epsilon_{m,xx}[e_{m,\alpha x}] - (\mathbf{q}_{m\alpha} \times [\mathbf{h}_{m,\alpha}])_x \right|^2 . \tag{3.19}$$

The solution to (3.18) can be easily found:

$$\mu_{m,xx} = \frac{\sum_\alpha (\mathbf{q}_{m\alpha} \times [\mathbf{e}_{m\alpha}])_x \, [h_{m,\alpha x}]^*}{k_0 \sum_\alpha \left| [h_{m,\alpha x}] \right|^2} , \tag{3.20}$$

where the asterisk denotes complex conjugation. Similar expressions hold for the the other two components of the permeability and for the dielectric permittivity, e.g.,

$$\epsilon_{m,xx} = \frac{\sum_\alpha (\mathbf{q}_{m\alpha} \times [\mathbf{h}_{m\alpha}])_x \, [e_{m,\alpha x}]^*}{k_0 \sum_\alpha \left| [e_{m,\alpha x}] \right|^2} . \tag{3.21}$$

We can give a physical interpretation of the above expressions by noting the following. If only one Bloch wave is used in the calculations, then the homogenization formulas involve the ratio of the electric and magnetic field amplitudes, i.e., the square of the so-called Bloch impedance. In the more realistic case of many Bloch waves, expressions (3.20), (3.21) contain ensemble averages of the individual Bloch impedances of the basis waves. The physical significance of Bloch impedance has been discussed in detail by Simovski in [1]. Also, in a recent conceptually close development, Lawrence *et al.* [26] have provided a thorough analysis of the impedance boundary conditions and emphasized their importance. The key novelty of the present paper is a new definition of an effective impedance that is optimized for a given range of illumination conditions.

The general solution to (3.16) for a non-diagonal tensor can be expressed in terms of two $6 \times n$ matrices, $\Psi_{m,DB}$ and $\Psi_{m,EH}$, whose columns α are equal to $k_0^{-1}\mathcal{K}_{m\alpha}\{\mathbf{H}^{(0)}_{m\alpha}, \mathbf{E}^{(0)}_{m\alpha}\}$ and

$\{\mathbf{E}^{(0)}_{m\alpha}, \mathbf{H}^{(0)}_{m\alpha}\}$, respectively. Then (3.16) is equivalent to the following minimization problem:

$$\mathcal{M}_{m,\mathrm{opt}} \;=\; \arg\min_{\mathcal{M}} F_m(\mathcal{M}), \qquad F_m(\mathcal{M}) \equiv \left\| \Psi_{m,DB} - \mathcal{M}\Psi_{m,EH} \right\|, \tag{3.22}$$

where the Frobenius matrix norm is implied. This is a classical least-squares problem with the solution

$$\mathcal{M}_{m,\mathrm{opt}} \;=\; \Psi_{m,DB}\, \Psi^{+}_{m,EH}\,. \tag{3.23}$$

Here '+' denotes the Moore-Penrose pseudoinverse. This is very similar to the expressions in our earlier publications [17–19], where the Ψ matrices had an analogous meaning but were not the same as here.

In practice, the minimization problem (3.22) is expected to be overdetermined (i.e. the number of basis functions will exceed the total number of degrees of freedom). Indeed, to each coordinate axis there corresponds a natural set of four basis waves (two opposite directions of propagation, times two independent polarizations). Thus for a generic 3D problem the basis will typically contain 12 waves traveling along the coordinate axes, plus possibly additional waves traveling in other directions, thereby far exceeding the dimension 6 of the material tensor.

4. Error estimation

Let $\{\mathbf{e}, \mathbf{h}\}$ be the exact field inside and outside a metamaterial block and let us use the methodology described above to construct the coarse-level field $\{\mathbf{E}, \mathbf{H}\}$. More precisely, for any fine-scale field written as a superposition (3.2) of basis waves within the material, we define the respective coarse-level field inside the metamaterial as (3.9), where $\{\mathbf{E}^{(0)}_{m\alpha}, \mathbf{H}^{(0)}_{m\alpha}\}$ are determined according to the procedure of the previous section. Outside of the material, $\{\mathbf{E}, \mathbf{H}\}$ are defined according to (3.6) as extensions of the actual far field to the whole space.

The $\{\mathbf{E}(\mathbf{r}), \mathbf{H}(\mathbf{r})\}$ field so defined is important for theoretical analysis but is not available in practice because the exact field and the corresponding expansion coefficients $c_{m\alpha}$ are not known. The computable quantity is the field $\{\mathbf{E}_{\mathcal{M}}(\mathbf{r}), \mathbf{H}_{\mathcal{M}}(\mathbf{r})\}$ that would exist, under the same given illumination conditions, around an equivalent body with the material tensors $\mathcal{M}_m$ obtained via our homogenization procedure. We are interested in estimating the difference between $\{\mathbf{E}_{\mathcal{M}}(\mathbf{r}), \mathbf{H}_{\mathcal{M}}(\mathbf{r})\}$ and the actual far field (2.2). (In the near field, one does expect substantial pointwise differences between the exact field rapidly fluctuating in the vicinity of the material interface and the smooth field $\{\mathbf{E}_{\mathcal{M}}(\mathbf{r}), \mathbf{H}_{\mathcal{M}}(\mathbf{r})\}$.)

Since, by construction, the auxiliary field $\{\mathbf{E}(\mathbf{r}), \mathbf{H}(\mathbf{r})\}$ is equal to the actual field in the far zone, we may as well estimate the difference

$$\delta_{EH} \;\equiv\; \{\mathbf{E}_{\mathcal{M}}(\mathbf{r}), \mathbf{H}_{\mathcal{M}}(\mathbf{r})\} - \{\mathbf{E}(\mathbf{r}), \mathbf{H}(\mathbf{r})\} \tag{4.1}$$

in the far field. To this end, we note that $\{\mathbf{E}_{\mathcal{M}}, \mathbf{H}_{\mathcal{M}}\}$ satisfies the same equations (3.5) as $\{\mathbf{E}(\mathbf{r}), \mathbf{H}(\mathbf{r})\}$ but without the δ-terms. One concludes that the field error δ_{EH} is due to these terms.

Both surface and volume errors have been minimized in the procedure described in the previous section. We omit a detailed analysis of the surface error, but the volume error remaining after minimization is given by the functional F_m introduced above, viz.

$$\chi \;=\; \max_{m} \left[F_m(\mathcal{M}_{m,\mathrm{opt}}) \right]\,. \tag{4.2}$$

where F_m is defined in (3.22). We will view the quantity χ defined above as an error indicator; one can expect that the effective parameters produced by Trefftz homogenization yield accurate scattering predictions if $\chi \ll 1$.

5. Numerical examples

We now apply Trefftz homogenization to three different examples of periodic media. The first two examples involve one-dimensional layered structures which admit an analytical solution to

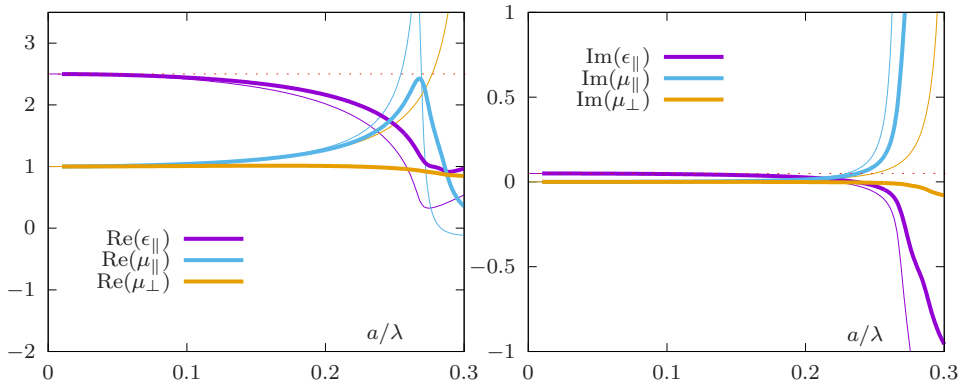

Figure 1. Example 1. Effective parameters by Trefftz homogenization (thick lines) and by S-parameter retrieval (thin lines) as functions of a/λ; the lattice period a changes while λ is fixed. The dotted line represents the classical homogenization limit for $\epsilon_\parallel$ (in s-polarization, the volume average of ϵ_1 and ϵ_2).

the electromagnetic problem. We use this fact to compare the exact transmission and reflection coefficients of a finite-width layered slab to predictions of the homogenization theory. The third example is a two-dimensional lattice of infinite dielectric cylinders. No analytical solution is available for this structure. Therefore we have used for comparison and validation purposes sixth-order finite difference FLAME schemes described in Refs. [24,25,27,28].

(a) Example 1: Layered dielectric medium

In Example 1, we consider a layered medium which is periodic in the Z direction and homogeneous in the XY plane. The medium consists of a finite number of stacked inversion-symmetric lattice cells. Each cell contains three intrinsically nonmagnetic layers of widths $a/4$, $a/2$ and $a/4$ and scalar permittivities ϵ_1, ϵ_2, and ϵ_1, respectively. The lattice period (the width of one elementary cell) is equal to a. In this example, we take $\epsilon_1 = 4 + 0.1i$ and $\epsilon_2 = 1$, that is, the outer layers of an elementary cell are made of an absorbing dielectric and the central layer is free space. Note that a finite-width structure of this kind is terminated by two dielectric layers of the width $a/4$ on each side. Each elementary cell and the composite as a whole has a center of symmetry, and consequently the effective material tensor is diagonal; in particular, there is no magnetoelectric coupling. In Example 1, we do not consider the effects of dispersion and assume that the variable a/λ can change while ϵ_1 and ϵ_2 are constant. This is physically achievable, for instance, if λ is fixed and a can change.

We present results for s-polarization (one-component electric field, two-component magnetic field); results for p-polarization are qualitatively similar. For s-polarization, the relevant elements of the effective permittivity and permeability tensors are $\epsilon_\parallel$, $\mu_\parallel$ and $\mu_\perp$, where the indexes $\parallel$ and $\perp$ indicate the directions along and perpendicular to the layers.

We start by considering the dependence of the effective parameters on the normalized cell size a/λ. The Trefftz basis used in this computation consisted of $2n$ Bloch waves with different tangential components of the wave vector, k_x (the incidence plane is XZ). The above factor of two accounts for the two possible directions of propagation along the Z-axis. We have observed that the numerical results depend very mildly on n as long as is $n \gtrsim 5$. Correspondingly, we have used $n = 7$.

In Fig. 1, we display the effective parameters obtained by Trefftz homogenization as well as by S-parameter retrieval method. A particular implementation of S-parameter retrieval described in Appendix C of Ref. [11] has been implemented (specifically, we have used Method 2 for $\epsilon_\parallel$ and $\mu_\parallel$ and Method 3 for $\mu_\perp$). For small and moderate values of the cell size ($a/\lambda \sim 0.15$), the agreement

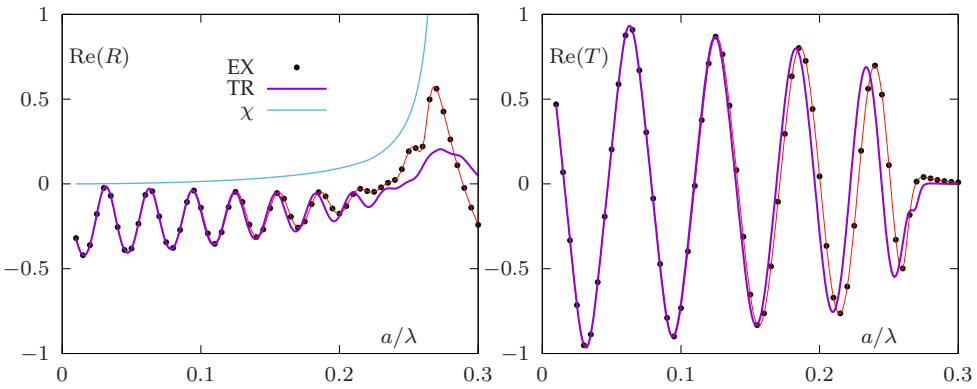

Figure 2. Example 1. Real parts of the reflection coefficient R (left) and transmission coefficient T (right), and the homogenization error indicator χ (4.2) (left) for the layered structure consisting of $L = 10$ elementary cells and for the equivalent homogenized slab as functions of a/λ. EX – exact results, TR – Trefftz homogenization.

between these two sets of results is almost perfect but beyond that point they diverge. This is not surprising because Trefftz homogenization optimizes effective parameters in a wide range of propagation angles while S-parameter retrieval optimizes transmission/reflection (T/R) only for a small range of near-normal incidence angles in the formulation of Ref. [11], which was used here.

We now compare the T/R coefficients computed exactly for a slab consisting of $L = 10$ elementary cells and for an equivalent homogenized slab of width $W = La$. Since the principal objective of homogenization is to predict transmission and reflection of waves, the discrepancy between these results is the best measure of the accuracy of the effective parameters obtained. It should be borne in mind, however, that errors in the transmitted wave (especially, phase errors) accumulate as that wave propagates through the slab; hence the error in the transmission coefficient will generally be higher for thicker samples, regardless of the homogenization methodology.

The reflection and transmission coefficients defined as the ratios of the complex amplitudes of the reflected/transmitted and incident tangential fields computed at the slab boundaries (the electric field for s-polarization) are plotted in Fig. 2 as functions of a/λ at normal incidence. We also show in the same plot the error indicator χ (4.2). It can be seen that the error indicator is relatively small for $a/\lambda \lesssim 0.2$ but grows rapidly and exceeds unity when $a/\lambda \gtrsim 0.2$. We can conclude that homogenization in Example 1 is accurate for $a/\lambda \lesssim 0.2$ and that the medium is not homogenizable (at least in terms of local parameters) for $a/\lambda \gtrsim 0.2$.

The data for Fig. 2 was produced using a Trefftz basis set of Bloch waves with the X-components k_x of the wave vector bounded as $|k_x| \le k_0$. This accounts for illumination by *propagating* waves. In applications related to imaging beyond the diffraction limit, one should also include in the basis Bloch waves with $|k_x| > k_0$, which corresponds to evanescent incident waves. Doing so is expected to further limit the range of a/λ where homogenization is accurate. However, in other applications, one may wish to tailor the effective parameters to a restricted range of incidence angles. By choosing a narrower range, one expects to improve the accuracy of the effective medium description at the expense of narrowing its range of applicability. This trade-off is illustrated next.

Specifically, we have restricted the set of basis functions so that $|k_x/k_0| < \sin\theta_{\max}$. We have applied Trefftz homogenization to produce effective parameters for different values of $\theta_{\max}$ and then used the homogenization result thus obtained to compute T/R in the whole range of incidence angles θ, that is, for $0 \le \theta \le \pi/2$. The T/R values computed in this manner are expected to be accurate only for $\theta \lesssim \theta_{\max}$. This is illustrated in Fig. 3 for $\theta_{\max} = \pi/10$ (left panel) and

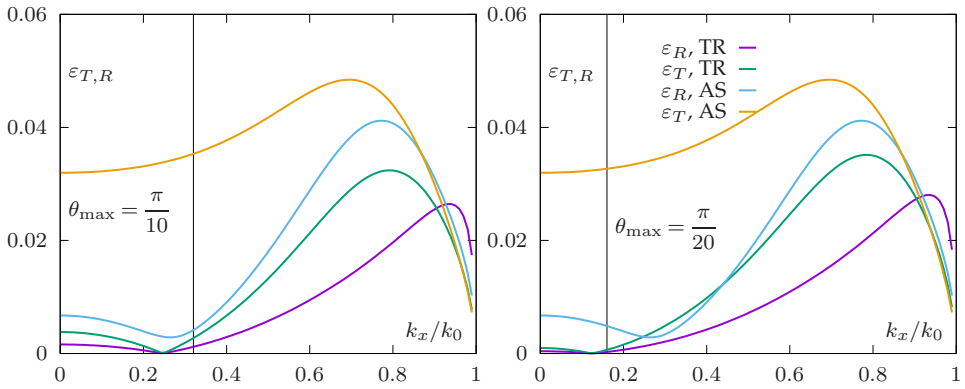

Figure 3. Example 1. Errors in the transmission and reflection coefficients (5.1) as functions of the sine of the incident angle, $\sin\theta = k_x/k_0$, for $a/\lambda = 0.2$. The errors are displayed for Trefftz homogenization (TR) and for the classical asymptotic homogenization limit (AS). The maximum angles of incidence in the restricted set of basis functions for Trefftz homogenization [$\theta_{\max} = \pi/10$ (left) and $\theta_{\max} = \pi/20$ (right)] are indicated by the vertical lines.

$\theta_{\max} = \pi/20$ (right panel). In this figure, the normalized cell size is fixed at $a/\lambda = 0.2$ and we display the errors in the transmission and reflection coefficients as functions of $\sin\theta = k_x/k_0$. The errors are defined as

$$\varepsilon_R \equiv |R_{\text{predicted}} - R_{\text{exact}}|\,, \quad \varepsilon_T \equiv |T_{\text{predicted}} - T_{\text{exact}}| \tag{5.1}$$

and should not be confused with the error indicator χ or with dielectric permittivity ϵ. Note that for $a/\lambda = 0.2$, $\chi = 0.093$, which makes this a borderline case for local homogenizability. For comparison, we also show in Fig. 3 the errors in T/R incurred by using the classical (quasi-static) homogenization limit, where $\mu = 1$ and ϵ is (for the s-mode) just the volume average of $\tilde{\epsilon}(\mathbf{r})$. It is evident from the figure that Trefftz homogenization predicts T/R with high accuracy in the range of its applicability $\theta < \theta_{\max}$ but may yield inaccurate T/E predictions outside of this range. By comparing the two values of $\theta_{\max}$ considered, we find that the errors *in the range of applicability* (which is, of course, different in these two cases) are much smaller for $\theta_{\max} = \pi/20$ than for $\theta_{\max} = \pi/10$. This trade-off between accuracy and the range applicability is a natural feature of Trefftz homogenization, and it can be demonstrated for all numerical examples considered below.

(b) Example 2: Dispersive layered metal-dielectric medium

In this example, the geometric parameters of the layered medium is the same as in Example 1, and we still consider s-polarization. However, we now assume that the second layer of the lattice cell is a dispersive metal whose permittivity is given by Drude formula

$$\epsilon_2 = \epsilon_{\text{int}} - \frac{\omega_p^2}{\omega(\omega + i\gamma)}\,, \tag{5.2}$$

where $\epsilon_{\text{int}} - 1$ is a contribution of interband transitions (assumed to be real and frequency-independent in the spectral range of interest), ω_p is the plasma frequency and γ is the Drude relaxation constant. The parameters used in simulations corresponded approximately to the experimental values for silver: $\epsilon_{\text{int}} = 5$ and $\omega_p/\gamma = 500$; $\lambda_p = 136$ nm. The lattice period is fixed at $a = 0.2\lambda_p$, where $\lambda_p = 2\pi c/\omega_p$ is the wavelength at the plasma frequency. Using the above values of parameters, we find that this corresponds to $a \approx 27$ nm. The free-space wavelength λ in this example varies and we fully account for the frequency dispersion by using Drude formula (5.2).

The effective parameters for example are plotted in Fig. 4 as functions of a/λ. The T/R data at normal incidence are plotted in Fig. 5 in a manner that is completely analogous to Fig. 2, except

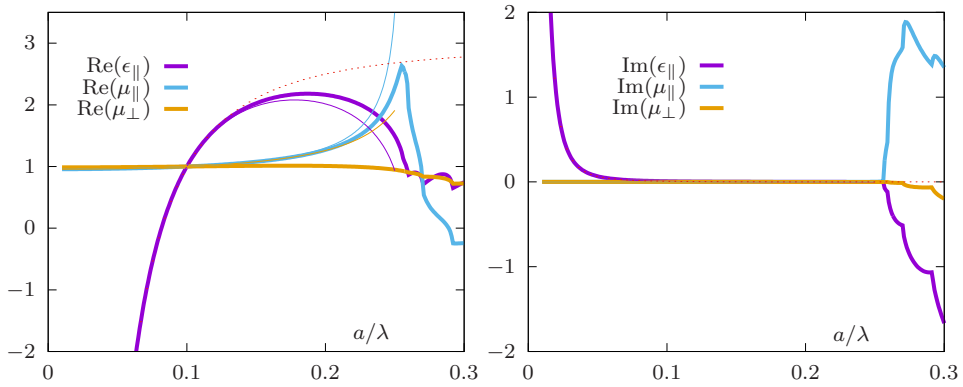

Figure 4. Example 2. Same as in Fig. 1 but for Example 2. The retrieval result is shown up to the point $a/\lambda = 0.25$, beyond which retrieval is numerically unstable. Note that in the right panel, Trefftz, retrieval and classical homogenization results are visually indistinguishable due to the large dynamic range of the data. However, these results are numerically different.

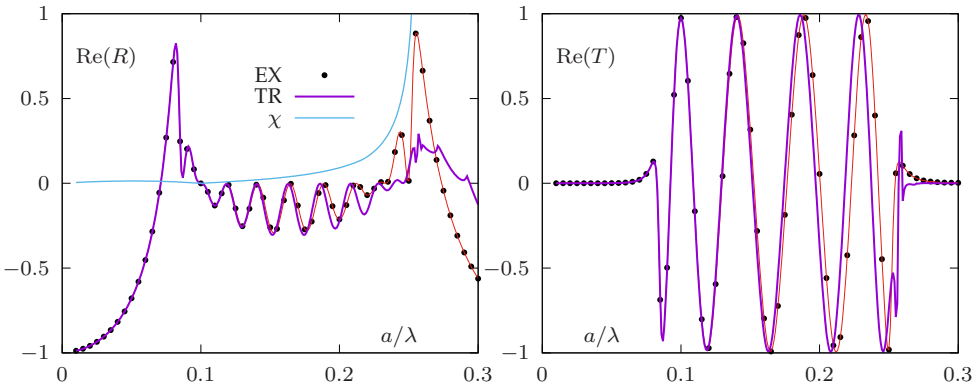

Figure 5. Example 2. Same as in Fig. 2 but for Example 2.

that now the parameter a/λ changes because λ varies while a is fixed. As before, the actual slab contained $L = 10$ elementary cells and we have used Trefftz basis restricted by $k_x \leq k_0$ to compute the effective parameters. It can be seen that the actual and homogenized slabs have approximately the same T/R in the limit $a/\lambda \to 0$, although the asymptotic behavior is in this case not as straightforward due to the effects of dispersion.

We finally show the same set of data as in Fig. 3 but with one modification. Namely, we consider here the Trefftz basis restricted to $\theta_{\max} = \pi/10$ in one case and to $\theta_{\max} = \pi/2$ in another (i.e., all propagating incident waves are included); restriction $\theta_{\max} = \pi/20$ is not used. The trade-off between the accuracy and range of applicability of the effective medium description is clearly visible from this figure. Indeed, the restriction $\theta_{\max} = \pi/10$ provides reasonable results in the range of its applicability but poor precision outside of this range. The restriction $\theta_{\max} = \pi/2$ (i.e. all propagating waves included) does not provide good approximation for any incidence angle, although Trefftz homogenization still yields uniformly smaller errors than the classical homogenization limit.

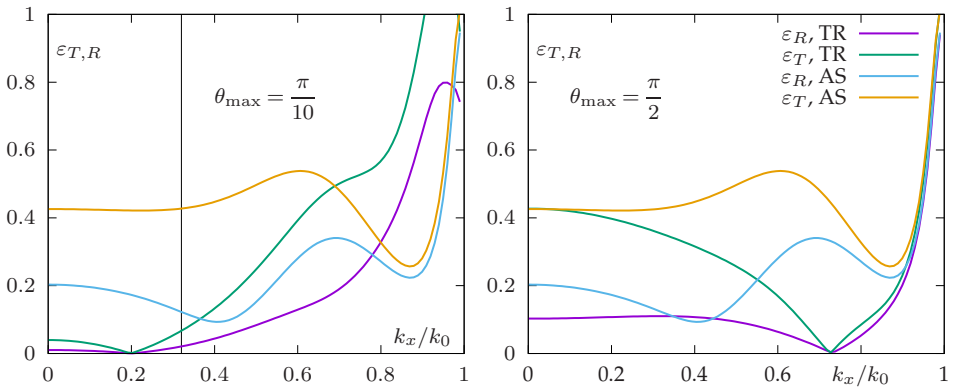

Figure 6. Example 2. Same as in Fig. 3 but for Example 2, with the following modification: The maximum angles of incidence in the restricted set of basis functions for Trefftz homogenization are $\theta_{\max} = \pi/10$ (left) and $\theta_{\max} = \pi/2$ (right). The normalized cell size is $a/\lambda = 0.2$.

(c) Example 3: A Periodic 2D array of cylinders.

We now consider a more complicated example which does not admit an analytical solution. Namely, Example 3 is a two-dimensional array of infinite dielectric cylinders illuminated by a p-polarized external wave. The radius of each cylinder is fixed at $r_{\rm cyl} = 0.33a$ and the dielectric permittivity of cylinders is $\epsilon_{\rm cyl} = 9.61$. The material of which the cylinders are made is assumed to be nonabsorbing and nondispersive in the spectral range of interest [2]. Under these conditions, the solution to the electromagnetic problem depends on the dimensionless ratio a/λ but not on a and λ separately. In p-polarization, the relevant component of the permittivity and permeability tensors are $\epsilon_{\|}$, $\epsilon_{\perp}$ and $\mu_{\|}$. The system is obviously electrically isotropic. Therefore, if we use Trefftz basis sets with the same underlying cubic symmetry, the effective parameters obtained are guaranteed to satisfy $\epsilon_{\|} = \epsilon_{\perp}$. However, if we use Trefftz basis sets that are not cubically-symmetric (e.g., due to a restriction of the incidence angles), the homogenization result can become electrically anisotropic. An example will be given below. This type of anisotropy is an effect of restricting the illumination conditions, not a violation of any physical principle. We finally note that the effective parameters in Example 3 are purely real.

Effective parameters obtained with different methods for Example 3 are shown in Fig. 7. In Trefftz homogenization, we used $\theta_{\max} = \pi/2$, i.e. all possible angles of propagation but excluding evanescent waves. A basis set with this property can be made cubically symmetric, which was indeed done in the simulations. The corresponding effective parameters were electrically isotropic. We also show in Fig. 7 the effective parameters obtained for the same structure by the two-dimensional Maxwell-Garnett approximation and by the asymptotic homogenization theory of Ref. [12].

We now use the effective parameters displayed in Fig. 7 to compute the transmission and reflection coefficients for a finite structure consisting of $L = 10$ layers of elementary cells and to compare T/R for the equivalent homogeneous slab to the exact results, which were obtained by the finite difference method previously referred to as FD-FLAME [24,25,27,28]. In p-polarization, the magnetic field has only one component. Therefore, the transmission and reflection coefficients are defined here as the ratios of the complex amplitudes of the magnetic field in the reflected/transmitted wave to that of the incident wave. In Fig. 8, we plot the real parts of R and T at normal incidence as functions of a/λ. It is evident that Trefftz homogenization is significantly more accurate than the asymptotic homogenization results,

[2] These parameters are the same as in [17,25,29]. In [29], the cylinders were Al_2O_3 rods in air and experiments were performed in the frequency range from 26 to 40GHz. We are using this setup as a generic benchmark only.

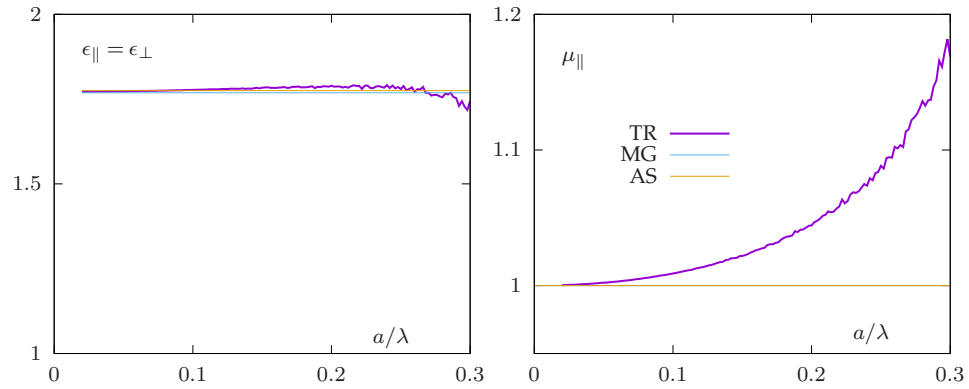

Figure 7. Example 3. Effective parameters for Example 3. TR – Trefftz homogenization , MG - Maxwell-Garnett, AS – asymptotic homogenization theory of Ref. [12]. All homogenization methods produce purely real ϵ and μ. In addition, the system is electrically isotropic due to the cubic symmetry of the underlying structure and of the Trefftz basis set, so that $\epsilon_{\|} = \epsilon_{\perp}$.

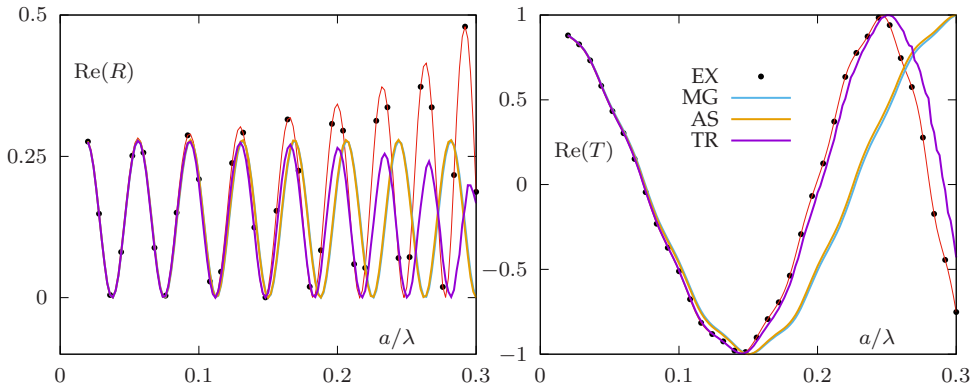

Figure 8. Example 3. Real parts of the reflection (left) and transmission (right) coefficient vs. a/λ at normal incidence. The curve labeled EX gives the accurate numerical result obtained by FD-FLAME. Different homogenization methods are labeled as follows: TR – Trefftz homogenization, MG – Maxwell-Garnett, AS – asymptotic homogenization of Ref. [12].

especially for transmission data. Nevertheless, the accuracy deteriorates for all methods at $a/\lambda \gtrsim 0.3$.

Next, we show data similar to that of Figs. 3 and 6 for Examples 1 and 2. Namely, we fix the ratio a/λ at $a/\lambda = 0.2$ and plot the errors in R/T for a $L = 10$ layered structure as a function of $k_x/k_0 = \sin\theta$, where θ is the incidence angle. As before, we use different restrictions on the Trefftz basis. The results are shown in Fig. 9. For comparison, we also plot the error for the asymptotic homogenization method of Ref. [12]. It can be seen that the restriction of the Trefftz basis $\theta_{\max} = \pi/10$ results in relatively small errors in the range of applicability of the homogenization theory, that is, for $\theta < \theta_{\max}$. Outside of this range, the errors increase rapidly (left plot in Fig. 9). In the case of the restriction $\theta_{\max} = \pi/2$ (right plot in Fig. 9), the range of applicability includes all propagating p-polarized incident waves, but not evanescent waves. It can be seen that the errors are in this case somewhat larger than in the case $\theta_{\max} = \pi/10$. However, the errors are distributed more evenly in the interval $0 < \theta < \pi/2$ $(0 < k_x < k_0)$ with a single pronounced spike near the

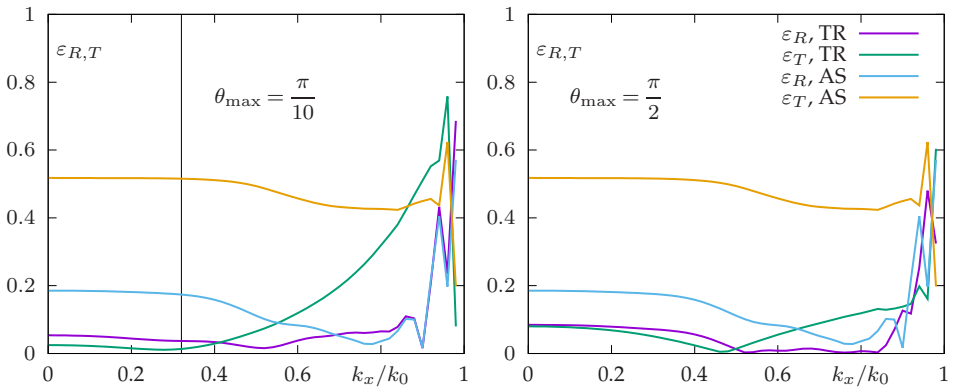

Figure 9. Example 3. Same as in Fig. 3 and Fig 6 but for Example 3 The maximum angles of incidence in the restricted set of basis functions for Trefftz homogenization are $\theta_{\max} = \pi/10$ (left) and $\theta_{\max} = \pi/2$ (right). The normalized cell size is $a/\lambda = 0.2$.

point $k_x = k_0$, which corresponds to grazing incidence. This behavior is expected and illustrates again the trade-off between the precision and the range of applicability of Trefftz homogenization.

We finally return to the question of isotropy of the effective parameters. Under general illumination conditions, our method produces material parameters perfectly consistent with the four-fold symmetry of the structure. However, restrictions on illumination can break that symmetry. This is not a contradiction since the problem of wave propagation and scattering involves not only the symmetric structure itself but also the external illumination. For restricted illumination conditions, an anisotropic material tensor can provide a better approximation of T/R data than an isotropic tensor would. For example, the effective permittivity computed for $a/\lambda = 0.2$ and the Trefftz basis restriction $\theta_{\max} = \pi/10$ are $\epsilon_\perp = 1.59$ and $\epsilon_\parallel = 1.86$. Note that the structure is expected to be magnetically anisotropic even for a symmetric Trefftz basis, but the component $\mu_\perp$ does not influence T/R data in p-polarization.

6. Summary and discussion

We have described a two-scale homogenization theory for periodic electromagnetic composites. The proposed methodology is nonasymptotic, which means that it does not involve any asymptotic expansions or mathematical limits with respect to any physical parameter of the composite or a combination thereof. Instead, we approximate the coarse-level and fine-level fields by expansions in a basis of local cell-wise functions that satisfy homogeneous Maxwell's equations. The expansion is accurate for a given range of illumination conditions. Once the fine-level basis set has been defined, the homogenization procedure is easy to implement, as it involves only the boundary averages of the tangential components of the basis functions and standard linear algebra. The residual error terms in Maxwell's equations serve as an error indicator. If its value is small, the homogenization results are accurate; otherwise, the periodic structure is not describable in terms of local effective parameters under the illumination conditions considered. Numerical results for several benchmark problems of layered media and a periodic array of cylinders illustrate the above points.

In the zero-cell-size limit, the new theory applies under any physical illumination conditions and yields the same results as classical two-scale asymptotic theories. For cells that are not vanishingly small, our analysis and numerical examples show that the new theory is more accurate than classical ones and applies under a well-defined range of illumination conditions where local homogenization is still feasible.

Approximation of fields near the material/air interface requires special consideration due to the presence of complicated surface waves that we have analyzed previously [12,13]; see also earlier papers by Felbacq and Simovski [1,2,30] and references therein. If a good approximation of surface waves with evanescent Bloch waves can be found, it can be integrated seamlessly into the homogenization procedure proposed in this paper.

In comparison with S-parameter retrieval, our methodology has a number of advantages. First, we optimize the effective parameters for a defined range of illuminating conditions, not just for one incident plane wave. Second, our approach results in a linear optimization problem whose solution is well understood in mathematics, unlike in the standard formulation of the nonlinear inverse problem of S-parameter retrieval. Third, our methodology allows one to define position-dependent parameters if needed.

We note that the mathematical tools used in this paper (in particular, Trefftz approximations) are rarely encountered in the literature on homogenization and therefore the analysis may appear abstractly mathematical. In fact, our development is driven by physical considerations and is designed to predict measurable quantities such as transmission and reflection coefficients. We have shown that this objective is achieved by our approach, subject to unavoidable approximation errors. Moreover, Trefftz approximations employed in our method have a clear physical meaning themselves – as a decomposition of fine-level and coarse-level fields into physical modes that can exist in the periodic composite (e.g., Bloch waves) and in the equivalent homogeneous medium (plane waves). Finally, Trefftz homogenization yields effective parameters that provide, in a sense, the best approximation of Bloch impedances as well as dispersion relations over an ensemble of physical modes in the structure.

In summary, the proposed methodology follows from physically relevant considerations and is both general and flexible. Information about the actual fine-scale fields is "encoded" in suitable sets of basis functions from which the effective material parameters are easily and unambiguously derived.

Acknowledgment

This research was supported by US National Science Foundation under Grant DMS-1216970.

References

1. C. R. Simovski. Material paremeters of metamaterials (a review). *Opt. Spectrosc.* **107**, 766–793, 2009.
2. C. R. Simovski. On electromagnetic characterization and homogenization of nanostructured metamaterials. *J. Opt.* **13**, 103001, 2011.
3. A. Bensoussan, J. L. Lions, and G. Papanicolaou. *Asymptotic Methods in Periodic Media*. North Holland, 1978.
4. G. Milton. *The Theory of Composites*. Cambridge University Press, 2002.
5. S. R. Arridge. Optical tomography in medical imaging. *Inverse Problems* **15**, R41–R93, 1999.
6. S. R. Arridge and J. C. Schotland. Optical tomography: forward and inverse problems. *Inverse Problems* **25**, 123010, 2009.
7. T. Koschny, P. Markos, D. R. Smith, and C. M. Soukoulis. Resonant and antiresonant frequency dependence of the effective parameters of metamaterials. *Phys. Rev. E* **68**, 065602(R), 2003.
8. X. Chen, T. M. Grzegorczyk, B. I. Wu, J. Pacheco, and J. A. Kong. Robust method to retrieve the constitutive effective parameters of metamaterials. *Phys. Rev. E* **70**, 016608, 2004.
9. S. Feng. Graphical retrieval method for orthorombic anisotropic materials. *Opt. Expr.* **18**, 17009–17019, 2010.
10. C. Menzel, C. Rockstuhl, T. Paul, F. Lederer, and T. Pertsch. Retrieving effective parameters for metamaterials at oblique incidence. *Phys. Rev. B* **77**, 195328, 2008.
11. V. A. Markel and I. Tsukerman. Current-driven homogenization and effective medium parameters for finite samples. *Phys. Rev. B* **88**, 125131, 2013.
12. V. A. Markel and J. C. Schotland. Homogenization of Maxwell's equations in periodic composites. *Phys. Rev. E* **85**, 066603, 2012.

13. X. Y. Z. Xiong, L. J. Jiang, V. A. Markel, and I. Tsukerman. Surface waves in three-dimensional electromagnetic composites and their effect on homogenization. *Opt. Expr.* **21**, 10412–10421, 2013.
14. J. B. Pendry. Negative refraction makes a perfect lens. *Phys. Rev. Lett.* **85**, 3966–3969, 2000.
15. R. V. Craster, J. Kaplunov, and A. V. Pichugin. High-frequency homogenization for periodic media. *Proc. Royal Soc. A* **466**, 2341–2362, 2010.
16. R. V. Craster, J. Kaplunov, E. Nolde, and S. Guenneau. Bloch dispersion and high frequency homogenization for separable doubly-periodic structures. *Wave Motion* **49**, 333–346, 2012.
17. I. Tsukerman. Effective parameters of metamaterials: a rigorous homogenization theory via Whitney interpolation. *J. Opt. Soc. Am. B* **28**, 577–586, 2011.
18. I. Tsukerman. Nonlocal homogenization of metamaterials by dual interpolation of fields. *J. Opt. Soc. Am. B* **28**, 2956–2965, 2011.
19. A. Pors, I. Tsukerman, and S. I. Bozhevolnyi. Effective constitutive parameters of plasmonic metamaterials: Homogenization by dual field interpolation. *Phys. Rev. E* **84**, 016609, 2011.
20. I. Herrera. Trefftz method: A general theory. *Numer. Meth. Part. Diff. Eq.* **16**, 561–580, 2000.
21. R. Hiptmair, A. Moiola, and I. Perugia. Error analysis of Trefftz-discontinuous Galerkin methods for the time-harmonic Maxwell equations. *Math. Comp.* **82**, 247–268, 2013.
22. A. Moiola. *Trefftz-Discontinuous Galerkin Methods for Time-Harmonic Wave Problems*. PhD thesis, ETH Zurich, 2011.
23. C. Scheiber, A. Schultschik, O. Bíró, and R. Dyczij-Edlinger. A model order reduction method for efficient band structure calculations of photonic crystals. *IEEE Trans. Magn.* **47**, 1534–1537, 2011.
24. I. Tsukerman. *Computational Methods for Nanoscale Applications: Particles, Plasmons and Waves*. Springer, 2007.
25. I. Tsukerman and F. Čajko. Photonic band structure computation using FLAME. *IEEE Trans. Magn.* **44**, 1382–1385, 2008.
26. F. J. Lawrence, C. M. de Sterke, L. C. Botten, R. C. McPhedran, and K. B. Dossou. Modeling photonic crystal interfaces and stacks: impedance-based approaches. *Adv. Opt. Photon.* **5**, 385–455, 2013.
27. I. Tsukerman. Electromagnetic applications of a new finite-difference calculus. *IEEE Trans. Magn.* **41**, 2206–2225, 2005.
28. I. Tsukerman. A class of difference schemes with flexible local approximation. *J. Comp. Phys.* **211**, 659–699, 2006.
29. R. Gajic, R. Meisels, F. Kuchar, and K. Hingerl. Refraction and rightness in photonic crystals. *Opt. Expr.* **13**, 8596–8605, 2005.
30. D. Felbacq. Anomalous homogeneous behaviour of metallic photonic crystals. *J. Phys. A* **33**, 815–821, 2000.

Appendix: Equations for coarse-level fields

Substituting expansion (3.9) into the coarse-field equations (3.5*a*), (3.5*b*), one obtains the following error term in the volume of each lattice cell:

$$-i\{\delta\mathbf{I}_m(\mathbf{r}),\delta\mathbf{J}_m(\mathbf{r})\}=\sum_\alpha c_{m\alpha}\left[\mathcal{K}_\alpha\{\mathbf{H}_\alpha^{(0)},\mathbf{E}_\alpha^{(0)}\}-k_0\mathcal{M}\{\mathbf{E}_\alpha^{(0)},\mathbf{H}_\alpha^{(0)}\}\right]\ ,\quad \mathbf{r}\in\mathbb{C}_m\ .$$

The error term corresponding to cell/cell boundaries is

$$\{\delta\mathbf{K}_{lm}(\mathbf{r}),\delta\mathbf{Q}_{lm}(\mathbf{r})\}=\hat{\mathbf{n}}_{lm}\times\sum_\alpha\{\mathbf{H}_\alpha^{(0)},\mathbf{E}_\alpha^{(0)}\}(c_{m\alpha}-c_{\alpha l})e^{i\mathbf{q}_\alpha\cdot\mathbf{r}}\ ,\quad \mathbf{r}\in\mathbb{S}_{lm}\ ,\ z\neq 0,L\ .$$

Finally, the error terms on the material/air interfaces are

$$\{\delta\mathbf{K}_{0m}(\mathbf{r}),\delta\mathbf{Q}_{0m}(\mathbf{r})\}=$$
$$\hat{\mathbf{z}}\times\left[\sum_\alpha c_{m\alpha}\{\mathbf{H}_\alpha^{(0)},\mathbf{E}_\alpha^{(0)}\}e^{i\mathbf{q}_\alpha\cdot\mathbf{r}}-\int\{\frac{\mathbf{k}_r}{k_0}\times\mathbf{S}_r(\mathbf{k}_r),\mathbf{S}_r(\mathbf{k}_r)\}e^{i\mathbf{k}_r\cdot\mathbf{r}}\,dk_{rx}\,dk_{ry}\right]\ ,$$
$$\mathbf{r}\in\mathbb{S}_{0m}\ ,\ z=0$$

on the side of the incident field and

$$\{\delta\mathbf{K}_{m\infty}(\mathbf{r}),\delta\mathbf{Q}_{m\infty}(\mathbf{r})\}=$$
$$\hat{\mathbf{z}}\times\left[\int\{\frac{\mathbf{k}_t}{k_0}\times\mathbf{S}_t(\mathbf{k}_t),\mathbf{S}_t(\mathbf{k}_t)\}e^{i\mathbf{k}_t\cdot\mathbf{r}}-\sum_\alpha c_{m\alpha}\{\mathbf{H}_\alpha^{(0)},\mathbf{E}_\alpha^{(0)}\}e^{i\mathbf{q}_\alpha\cdot\mathbf{r}}\,dk_{rx}\,dk_{ry}\right]\ ,$$
$$\mathbf{r}\in\mathbb{S}_{m\infty}\ ,\ z=L$$

on the transmission side. In these expressions, k_z is a function of k_x and k_y defined by the free-space dispersion formula (2.3) and, finally,

$$\mathbf{k}_t=(k_x,k_y,k_z)\ ,\quad \mathbf{k}_r=(k_x,k_y,-k_z)\ .$$